

Hamiltonian Monte Carlo using an embedded Laplace approximation

Charles C. Margossian^{*}, Aki Vehtari[†], Daniel Simpson[‡], and Raj Agrawal[§]

Abstract. Latent Gaussian models are a popular class of hierarchical models with applications in many fields. Performing Bayesian inference on such models can be challenging. Markov chain Monte Carlo algorithms struggle with the geometry of the resulting posterior distribution and can be prohibitively slow. An alternative is to use an integrated nested Laplace approximation, whereby we marginalize out the latent Gaussian variables and estimate the hyperparameters with a deterministic scheme. This type of inference typically only works for low dimensional and unimodal hyperparameters. We bypass these limitations by coupling dynamic Hamiltonian Monte Carlo with an embedded Laplace approximation. Our implementation features a novel adjoint method to differentiate the marginal likelihood, which scales with high dimensional hyperparameters. We prototype the method in the probabilistic programming framework Stan and test the utility of the embedded Laplace approximation on several models: a classic Gaussian process, a general linear regression model with a sparsity inducing horseshoe prior, and a sparse kernel interaction model. The last two models are characterized by a high dimensional and a multimodal posterior distribution of the hyperparameters, and as such present novel applications of the embedded Laplace approximation. Depending on the cases, the benefits are either a dramatic speed-up, or an alleviation of the geometric pathologies that frustrate Hamiltonian Monte Carlo.

Keywords— Hamiltonian Monte Carlo, Laplace approximation, automatic differentiation, latent Gaussian models, Bayesian inference

1. INTRODUCTION

Latent Gaussian models observe the following hierarchical structure:

$$\begin{aligned}\phi &\sim \pi(\phi) \\ \theta &\sim \text{Normal}(0, K(\phi)) \\ y &\sim \pi(y \mid \theta, \phi).\end{aligned}$$

Contact author: Charles Margossian

email: charles.margossian@columbia.edu

^{*}Department of Statistics, Columbia University

[†]Department of Computer Science, Aalto University

[‡]Department of Statistical Sciences, University of Toronto

[§]CSAIL, Massachusetts Institute of Technology

Typically, single observations y_i are independently distributed and only depend on a subset of the latent variables, that is $\pi(y_i \mid \theta, \phi) = \pi(y_i \mid a_i^T \theta, \phi)$, for some appropriately defined vectors a_i . This general framework finds a broad array of applications: Gaussian processes, spatial models, general linear models, and multilevel regression and post-ratification models to name a few examples. Our goal is to perform full Bayesian inference on θ and ϕ . We denote θ the *latent Gaussian variable* and ϕ the *hyperparameter*, although we note that in general ϕ denotes any latent variable other than θ . In some fields, θ is termed the random effect and ϕ the fixed effect.

1.1 Motivating problems

There are many types of latent Gaussian models that exhibit different behaviors. A classic example is Gaussian processes with a squared exponential kernel. Here, the covariance matrix K depends on the covariates x , which encode the location (geographical, temporal, or otherwise)

of the observation y , and two parameters, α and ρ , that respectively control the global standard deviation and the length scale. In this setup, $\phi = (\alpha, \rho)$ is two-dimensional. On the other hand, θ has the same dimension as y and is potentially high dimensional.

Next, consider the case of a high dimensional generalized linear regression. In many applications, the number of covariates, and hence the number of elements in the regression coefficient, β , exceeds the number of observations. We can fit such models by using a sparsity inducing prior, such as the regularized horseshoe prior (Piironen and Vehtari, 2017), which requires a high dimensional hyperparameter, ϕ (e.g. regularized linear regression (Piironen and Vehtari, 2017) and sparse kernel interaction models (Agrawal et al., 2019)). This problem can be recast as a latent Gaussian model. Unlike the Gaussian process example, both the latent Gaussian variable and the hyperparameters are high dimensional. What is more, several geometric challenges arise when examining the posterior distribution, such as high curvature and multimodality.

1.2 Existing methods

To perform Bayesian analysis, the algorithmic landscape is broadly speaking split between two approaches: (i) sampling schemes that generate an approximate sample from the posterior distribution using Markov chains Monte Carlo (MCMC), and (ii) variational methods in which one finds a tractable distribution that approximates the posterior. The same holds for latent Gaussian models, where we can consider Hamiltonian Monte Carlo (HMC) sampling (Neal, 2012; Betancourt, 2018a) or marginalizing out the latent Gaussian variables with a Laplace approximation before deterministically integrating the hyperparameters (Tierney and Kadane, 1986; Rue and Chopin, 2009).

Hamiltonian Monte Carlo sampling

When using MCMC sampling, the target distributions is

$$\pi(\theta, \phi | y) \propto \pi(y | \theta, \phi) \pi(\theta | \phi) \pi(\phi)$$

and the Markov chain explores the joint parameter space of θ and ϕ . Note that a sample from the joint distribution also produces a sample from the marginal distribution, $\pi(\phi | y)$, should we be primarily interested in ϕ .

HMC is a class of MCMC algorithms that powers many modern probabilistic programming languages, including Stan (Carpenter et al., 2017), PyMC3 (Salvatier, Wiecki and Fonnesbeck, 2016), and TensorFlow Probability¹. Its success is both empirically and theoretically motivated (e.g. Betancourt et al., 2017), and, amongst other things, lies in its ability to probe the geometry of the target distribution via the gradient. HMC scales in high-dimension, can sample strongly correlated variables and resolve multimodality, provided the energy barrier is not too strong.

¹<https://www.tensorflow.org/probability>

The algorithm is widely accessible through its dynamic variants, the No-U-Turn Sampler (Hoffman and Gelman, 2014) and the more recent version detailed by Betancourt (2018a), which spare the users the cumbersome task of manually setting the algorithm’s tuning parameters. In addition, *automatic differentiation* efficiently evaluates derivatives and alleviates the burden of calculating gradients by hand (for reviews on the subject in statistics and machine learning, we recommend Margossian (2019) and Baydin et al. (2018); for a more extensive treatment, the reader may consult Griewank and Walther (2008)). There are known challenges when applying HMC to hierarchical models (e.g. Betancourt and Girolami, 2013). Generally speaking, these problems are due to uneven scale in the parameter space, caused by varying correlation between parameters, and Neal’s (2003) infamous funnel. In the case of latent Gaussian models, this geometric grief is often caused by the latent Gaussian variable, θ , and its interaction with ϕ .

Marginalization using a Laplace approximation

The embedded Laplace approximation is also a very successful algorithm, and the main inference engine of the popular R packages INLA (*integrated nested Laplace integration*, Rue et al., 2017) and TMB (*template model builder*, Kristensen et al., 2016), and the Matlab package GPstuff (Vanhatalo et al., 2013). The idea is to marginalize out θ and then use standard inference techniques on ϕ . To do so, consider the factorization

$$\pi(\phi | y) \propto \frac{\pi(\phi) \pi(\theta | \phi) \pi(y | \theta, \phi)}{\pi(\theta | \phi, y)}.$$

We perform the Laplace approximation

$$\pi(\theta | \phi, y) \approx \pi_{\mathcal{G}}(\theta | y, \phi) := \text{Normal}(\theta^*, \Sigma^*),$$

where θ^* matches the mode and $[\Sigma^*]^{-1}$ the curvature of $\pi(\theta | \phi, y)$. Then

$$\pi(\phi | y) \approx \pi_{\mathcal{G}}(\phi | y) := \pi(\phi) \frac{\pi(\theta^* | \phi) \pi(y | \theta^*, \phi)}{\pi_{\mathcal{G}}(\theta^* | \phi, y)}.$$

The success of this scheme depends on how good the approximation is and requires $\pi(y | \theta, \phi)$ to be unimodal and well characterized by the curvature at its mode (Tierney and Kadane, 1986). Once we perform inference on ϕ , we can recover θ using the conditional distribution $\pi(\theta | \phi, y)$ and effectively marginalizing ϕ out. For certain models, this approach yields comparably accurate and much faster inference than MCMC (Rue and Chopin, 2009). Furthermore the Laplace approximation as a marginalization scheme has very good theoretical properties (e.g. Tierney and Kadane, 1986), and has been successfully used and verified in a wide variety of contexts (e.g. Rue et al., 2017; Botond and Heskes, 2011; Rasmussen and Williams, 2006).

In the R package INLA, approximate inference is performed on ϕ , by characterizing $\pi(\phi | y)$ around its presumed mode. This works well for many cases but presents two limitations: the posterior must be well characterized in the neighborhood of the estimated mode and it must be low dimensional, “2 - 5, not more than 20” (Rue et al., 2017). In one of our motivating examples, the posterior of ϕ is both high dimensional (~ 6000) and multimodal.

Hybrid methods

Naturally we can use a more flexible inference method on ϕ such as a standard MCMC, as discussed by Gómez-Rubio and Rue (2018), and HMC as proposed in GPstuff and TMB, the latter through its extension TMBStan and AdNuts (*automatic differentiation with a No-U-Turn Sampler*, Monnahan and Kristensen, 2018). The target distribution of the MCMC sampler is

$$\pi_G(\phi | y)$$

and samples from $\pi_G(\theta | y)$ are obtained in post-process, by simulating from $\pi_G(\theta | \phi, y)$ across the sampled ϕ 's. Thus the hybrid method solves an approximation of the original problem, the hope being that this approximation gives similar results but is easier to solve.

Using HMC incurs an important computational cost because the sampler requires the gradient of $\log \pi_G(y | \phi)$ with respect to ϕ . When differentiating the marginal likelihood, much care must be taken to insure efficient computation. TMB and GPstuff exemplify two approaches to differentiate the approximate marginal density. The first uses automatic differentiation and the second adapts the algorithms in Rasmussen and Williams (2006). One of the main bottlenecks is differentiating

$$\theta^*(\phi) = \underset{\theta}{\operatorname{argmax}} \pi(\theta | \phi, y).$$

In theory, it is straightforward to apply automatic differentiation, by brute-force propagating derivatives through θ^* , i.e. sequentially differentiating the iterations of a numerical optimizer. But this approach, termed the *direct method*, is prohibitively expensive. A much faster alternative is to use the implicit function theorem (e.g. Bell and Burke, 2008; Margossian, 2019). Given any accurate numerical solver, we can always use the implicit function theorem to get derivatives, as notably done in the Stan Math Library and in TMB's *inverse subset algorithm* (Kristensen et al., 2016). One side effect is that the numerical optimizer is treated as a black box. By contrast, Rasmussen and Williams (2006) define a bespoke Newton method to compute θ^* , meaning we can store relevant variables from the final Newton step when computing derivatives. In our experience, this leads to important computational savings. But overall this method is much less flexible, working well only when ϕ is low dimensional and requiring the user to

pass the tensor of derivatives

$$K' = \frac{\partial K}{\partial \phi},$$

and specify derivatives for the likelihood, $\pi(y | \theta, \phi)$.

1.3 Aim and results of the paper

We improve the computation of HMC with an embedded Laplace approximation and present an implementation that verifies the following: the algorithm can accommodate any covariance matrix K , efficiently differentiate $\log \pi_G(y | \phi)$, even when ϕ is high dimensional, handle any prior on ϕ and use dynamic HMC. We introduce an adjoint method to differentiate $\log \pi_G(y | \phi)$, build the algorithm in C++, and add it to the Stan language. Our approach builds on the bespoke Newton solver proposed by Rasmussen and Williams (2006) and also uses automatic differentiation. We find that, for the classic Gaussian process in Section 3, the computation time required to differentiate the marginal is on par with GPstuff. The adjoint method is however orders of magnitude faster when ϕ is high dimensional; see Section 2.5.

Equipped with this implementation, we test dynamic HMC with an embedded Laplace approximation on a range of models, including ones with a high dimensional and multimodal hyperparameter. We do so by benchmarking our implementation against Stan's dynamic HMC, which runs MCMC on both the hyperparameter and the latent Gaussian variable. For the rest of the paper, we call this standard use of dynamic HMC, *full HMC*. We refer to marginalizing out θ and using dynamic HMC on ϕ , as the (*embedded*) *Laplace approximation*.

The utility of coupling the Laplace approximation with HMC has been rightfully questioned. Monnahan and Kristensen (2018) examine two cases using TMBStan, an R package that interfaces TMB with Stan. In their first example, $\dim(\phi) = 3$ and $\dim(\theta) = 172$, but the speed-up is minor (26% faster than full HMC) and in their second model, the induced error is significant. The README file of TMBStan states using a Laplace approximation is “generally not recommended”². Our computer experiments shed more light on the matter and identify cases where the benefits, as tested with our implementation, are substantial. These benefits are either an important computational speed-up or an improved geometry of the posterior, which means the sampler requires no manual tuning.

In the classic case of a Gaussian process, the speed-up, compared to full HMC is an order of magnitude. We next examine a sparse linear regression model with a horseshoe prior applied to classification data for prostate cancer. Full HMC struggles with the posterior's geometry, as indicated by *divergent transitions* and requires a proper reparameterization and careful tuning. On the

²<https://github.com/kaskr/tmbstan>

other hand, the embedded Laplace approximation evades many of the geometric problems and solves the approximate problem efficiently. We find this to be true, even when $\text{dimension}(\theta) \sim 100$ and $\text{dimension}(\phi) \sim 6000$. This means the geometric benefits do not simply come from reducing the dimension of the parameter space MCMC explores, but truly from removing the latent Gaussian variables, which in this hierarchical setting are responsible for the pathological geometry. We obtain similar results when fitting a sparse kernel interaction model, which looks at second-order interactions between covariates.

In all the studied cases, the likelihood is log-concave. Detailed analysis on the error introduced by the Laplace approximation for log-concave likelihoods can be found in references (Kuss and Rasmussen, 2005; Vanhatalo, Pietiläinen and Vehtari, 2010; Botond and Heskes, 2011; Vehtari et al., 2016) and are consistent with the results from our computer experiments.

2. IMPLEMENTATION FOR PROBABILISTIC PROGRAMMING

In order to run HMC, we need a function that returns the approximate log density of the marginal likelihood, $\log \pi_{\mathcal{G}}(y | \phi)$ and its gradient with respect to ϕ , $\nabla \log \pi_{\mathcal{G}}(y | \phi)$. The user specifies the observations, y (or a sufficient statistic thereof), and a function to generate the covariance K , based on input covariates x and the hyperparameters ϕ . In the current prototype, the user picks the likelihood, $\pi(y | \theta, \phi)$ from a set of options³: for example, a Bernoulli distribution with a logit link.

The seminal book by Rasmussen and Williams (2006) details three algorithms, which respectively produce:

1. the mode θ^* and the approximate log marginal density $\log \pi_{\mathcal{G}}(y | \phi)$ (Algorithm 1),
2. the gradient, $\nabla \log \pi_{\mathcal{G}}(y | \phi)$ (Algorithm 2),
3. and simulations from $\pi_{\mathcal{G}}(\theta | y, \phi)$.

These are well-established methods. We use Algorithm 1 practically as is, but our differentiation algorithm is new. In this article, we will derive the latter as a correction to Algorithm 2. Our simulation method is mathematically equivalent to item 3 above and computationally comparable.

2.1 Evaluating the log marginal density

Algorithm 1 is a carefully constructed Newton solver. As a convergence criterion we use the change in the “objective function” between two iterations,

$$\Delta \log \pi(\theta | y, \phi) \leq \epsilon$$

³ Allowing the user to specify their own likelihood is on our to-do list; one major challenge is that we need to efficiently compute third-order derivatives.

for some ϵ^4 . We store many of the variables generated during the final Newton step to use them again when we compute the derivatives.

Algorithm 1 *Newton solver for the Laplace approximation*, algorithm 3.1 by Rasmussen and Williams (2006)

input: $K, y, \pi(y | \theta, \phi)$
 2: $\theta^* = \theta_0$ (initialization)
repeat
 4: $W = -\nabla \nabla \log \pi(y | \theta^*, \phi)$
 $L = \text{Cholesky}(I + W^{\frac{1}{2}} K W^{\frac{1}{2}})$
 6: $b = W \theta^* + \nabla \log \pi(y | \theta^*, \phi)$
 $a = b - W^{\frac{1}{2}} L^T \setminus (L \setminus (W^{\frac{1}{2}} K b))$
 8: $\theta^* = K a$
until convergence
 10: $\log \pi(y | \phi) = -\frac{1}{2} a^T \theta^* + \log \pi(y | \theta^*, \phi) - \sum_i \log L_{ii}$
return: $\theta^*, \log \pi_{\mathcal{G}}(y | \phi)$

2.2 Automatic differentiation

To compute the gradient $\nabla \log \pi_{\mathcal{G}}(y | \phi)$, we exploit several important principles of automatic differentiation. While widely used in statistics and machine learning, these principles remain arcane to many practitioners and deserve a brief review.

Given a composite map

$$f = f^L \circ f^{L-1} \circ \dots \circ f^1,$$

the chain rule teaches us that the corresponding Jacobian matrix observes a similar decomposition:

$$J = J_L \cdot J_{L-1} \cdot \dots \cdot J_1.$$

Based on computer code to calculate f , a *sweep of forward mode* automatic differentiation numerically evaluates the action of the Jacobian matrix on the initial tangent u , or *directional derivative* $J \cdot u$. Extrapolating from the chain rule

$$\begin{aligned} J \cdot u &= J_L \cdot J_{L-1} \cdot \dots \cdot J_3 \cdot J_2 \cdot J_1 \cdot u \\ &= J_L \cdot J_{L-1} \cdot \dots \cdot J_3 \cdot J_2 \cdot u_1 \\ &= J_L \cdot J_{L-1} \cdot \dots \cdot J_3 \cdot u_2 \\ &\dots \\ &= J_L \cdot u_{L-1}, \end{aligned}$$

where the u_l 's verify the recursion relationship

$$\begin{aligned} u_1 &= J_1 \cdot u \\ u_l &= J_l \cdot u_{l-1}. \end{aligned}$$

⁴ An alternative is to inspect $|\nabla_{\theta} \log \pi(\theta | y, \phi)|$. While more robust, this approach is costly, because unlike the log density, we do not get the gradient for free.

If our computation follows the steps outlined above we never need to explicitly compute the full Jacobian matrix, J_l , of an intermediate function, f^l ; rather we only calculate a sequence of Jacobian-tangent products.

Similarly a *reverse mode sweep* computes the action of a transposed cotangent on a Jacobian matrix $w^T J$. Which mode to choose depends on the type of derivatives we require. For example, if we wish to compute a Jacobian matrix for

$$f : \mathbb{R}^p \rightarrow \mathbb{R}^n,$$

we can obtain the derivatives with either p forward sweeps, initialized with p tangents, or n reverse sweeps, initialized with n cotangents.

2.3 Algorithm 2 using automatic differentiation

The main difficulty with Algorithm 2 from [Rasmussen and Williams \(2006\)](#) is the requirement for

$$\frac{\partial K}{\partial \phi_j}$$

at line 8. For classic problems, where K is, for instance, a squared exponential kernel, the derivatives are available analytically. This is of course not the case in general and we want a method that does not require the user to specify the tensor of derivatives, $\partial K/\partial \phi$.

Algorithm 2 *Gradient of the approximate marginal density, $\pi_{\mathcal{G}}(y | \phi)$, with respect to the hyperparameters ϕ* , adapted from algorithm 5.1 by [Rasmussen and Williams \(2006\)](#). The matrix of derivatives K' is highlighted in red. Note that all the operations on K' are linear.

input: $y, \phi, \pi(y | \theta, \phi)$
2: saved input from Algorithm 1: $\theta^*, K, W^{\frac{1}{2}}, L, a$
 $Z = \frac{1}{2} a^T \theta^* + \log \pi(y | \theta^*, \phi) - \sum \log(\text{diag}(L))$
4: $R = W^{\frac{1}{2}} L^T \setminus (L \setminus W^{\frac{1}{2}})$
 $C = L \setminus (W^{\frac{1}{2}} K)$
6: $s_2 = -\frac{1}{2} \text{diag}(\text{diag}(K) - \text{diag}(C^T C)) \nabla^3 \log \pi(y | \theta^*, \phi)$
for $j = 1 \dots \text{dim}(\phi)$
8: $K' = \partial K / \partial \phi_j$
 $s_1 = \frac{1}{2} a^T K' a - \frac{1}{2} \text{tr}(R K')$
10: $b = K' \nabla \log \pi(y | \theta, \phi)$
 $s_3 = b - K R b$
12: $\frac{\partial}{\partial \phi_j} \log \pi(y | \phi) = s_1 + s_2^T s_3$
end for
14: return $\nabla_{\phi} \log \pi_{\mathcal{G}}(y | \phi)$

Fortunately, automatic differentiation allows us to numerically evaluate $\partial K/\partial \phi$. To do this, we introduce the map \mathcal{K}

$$\begin{aligned} \mathcal{K} &: \mathbb{R}^p \rightarrow \mathbb{R}^{n(n+1)/2} \\ &\phi \rightarrow K, \end{aligned}$$

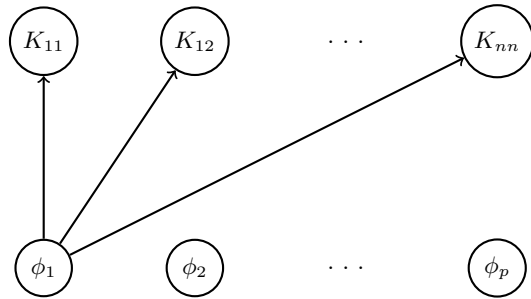


FIG 1. *Forward mode automatic differentiation of K . Starting with an initial tangent at ϕ_1 , one forward sweep through the expression graph computes the derivative of each element of K with respect to ϕ_1 . To get all the wanted derivatives and compute K' , the process must be repeated p times.*

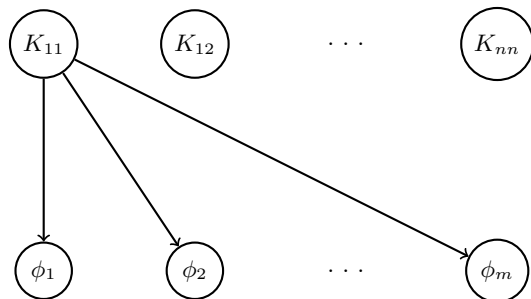


FIG 2. *Reverse mode automatic differentiation of K . Starting with an initial cotangent at K_{11} , one reverse sweep through the expression graph computes the derivative of K_{11} with respect to each element of ϕ . The process must be repeated $n(n+1)/2$ times to evaluate K' .*

where p is the dimension of ϕ and n that of θ . Based on computer code to evaluate K , automatic differentiation constructs an expression graph of the map \mathcal{K} and propagates derivatives through the operations on the graph, essentially applying the chain rule. A forward sweep starts with an initial tangent at the inputs, for instance 1 for one input and 0 for the other inputs, and propagates derivatives forwards. Given there are p inputs, we need p sweeps to compute $\partial K/\partial \phi$ (figure 1). A reverse sweep starts with an initial adjoint or cotangent at the outputs, for example 1 for one output and 0 for the other outputs, and propagates derivatives backward. We require n^2 , or exploiting the symmetry of K , $n(n+1)/2$ sweeps (figure 2). Given the scaling, we favor forward mode, and this works well when p is small. However when p becomes large, this approach fails spectacularly.

2.4 Adjoint method for the approximate log marginal density

Taking a step back, we recall that our goal is not to compute $\partial K/\partial\phi$ but $\nabla \log \pi_{\mathcal{G}}(y \mid \phi)$; and furthermore that automatic differentiation need not explicitly compute the Jacobian matrix of intermediate operations when differentiating a function. Per this logic, we should aim to build a method that differentiates $\log \pi_{\mathcal{G}}(y \mid \phi)$ in one reverse mode sweep without computing $\partial K/\partial\phi$. This type of reasoning plays a key role when differentiating functionals of implicit functions – for example, probability densities that depend on solutions to ordinary differential equations – and leads to so-called *adjoint methods* (e.g. [Errico, 1997](#)).

As motivated by our discussion on automatic differentiation, it is possible to evaluate the desired gradient with respect to ϕ using the right initial cotangent, w , and compute

$$w^T K'$$

in one reverse mode sweep. Standard applications of automatic differentiation, as alluded to in the introduction, such as the direct method or ones based on an implicit function theorem compute the derivatives in one sweep but they fail to exploit the structure of the problem, in contrast with Algorithm 2. We can get the best of both worlds with the following:

THEOREM 1. *Let $\log \pi_{\mathcal{G}}(y \mid \phi)$ be the approximate log marginal density in the context of a latent Gaussian model. Let a be defined as in Algorithm 1, and let R and s_2 be defined as in Algorithm 2. Then*

$$\nabla \log \pi_{\mathcal{G}}(y \mid \phi) = w^T \frac{\partial K}{\partial \phi}$$

where the gradient is with respect to ϕ and

$$w^T = \frac{1}{2}aa^T - \frac{1}{2}R + (s_2 + RKs_2)[\nabla_{\theta} \log \pi(y \mid \theta, \phi)]^T.$$

The proof follows from Algorithm 2 and noting that all the operations in K' are linear. We provide the details in Appendix A. Armed with this result, we build Algorithm 3.

2.5 Evaluation and comparison

We measure the time required for one evaluation and differentiation of $\log \pi_{\mathcal{G}}(y \mid \phi)$ for the sparse kernel interaction model developed by [Agrawal et al. \(2019\)](#) on simulated data. Note that the covariance matrix is far from trivial, hence the analytical solution is not available (see Appendix C.2). We simulate a range of data sets for varying dimensions, p , of ϕ . For low dimensions, the difference is small; however, for $p = 200$, Algorithm 3 is more than 100 times faster than Algorithm 2, requiring 0.009 s, rather 1.47 s. See Figure 3.

Algorithm 3 *Gradient of the approximate marginal log density, $\log \pi_{\mathcal{G}}(y \mid \phi)$, with respect to the hyperparameters, ϕ , using reverse mode automatic differentiation and theorem 1.*

- input:** $y, \phi, \pi(y \mid \theta, \phi)$
 2: Do lines 2 - 6 of Algorithm 2.
 Initiate an expression graph for automatic differentiation with $\phi_v = \phi$.
 4: $K_v = \mathcal{K}(\phi_v)$
 $w^T = \frac{1}{2}aa^T - \frac{1}{2}R + (s_2 + RKs_2)[\nabla_{\theta} \log \pi(y \mid \theta, \phi)]^T$
 6: Do a reverse sweep over K , with w as the initial cotangent to obtain $\nabla_{\phi} \log \pi_{\mathcal{G}}(y \mid \phi)$.
return: $\nabla_{\phi} \log \pi_{\mathcal{G}}(y \mid \phi)$.
-

3. GAUSSIAN PROCESS

A standard application of the embedded Laplace approximation is Gaussian processes. We fit the disease map of Finland by [Vanhatalo, Pietiläinen and Vehtari \(2010\)](#) which models the mortality count across the country. The data is aggregated in $n = 911$ counties. We use 100 counties, which allows us to fit the model quickly both with full HMC and HMC using an embedded Laplace approximation. For the i^{th} region, we have a 2-dimensional coordinate x_i , the counts of deaths y_i , and the standardized expected number of deaths, y_e^i . The covariance matrix is obtained using the squared exponential kernel

$$k(x_i, x_j) = \alpha^2 \exp\left(-\frac{(x_i - x_j)^T(x_i - x_j)}{\rho^2}\right),$$

where α is the marginal standard deviation and ρ the characteristic length scale. These constitute our hyperparameter ϕ . Note that analytical derivatives are built in the Stan library for this covariance matrix and can be incorporated in our differentiation scheme. The full latent Gaussian model is

$$\begin{aligned} (\rho, \alpha) &\sim \pi(\rho, \alpha) \\ \theta &\sim \text{Normal}(0, K(\alpha, \rho, x)) \\ y_i &\sim \text{Poisson}(y_e^i e^{\theta_i}). \end{aligned}$$

Fitting this model with MCMC requires running the Markov chains over all the parameters and latent variables, that is α , ρ , and θ . Because the data per group is sparse – one observation per group – the above hierarchical data generating process can lead to problematic geometries. The joint distribution between θ and α can have a funnel shape, with a high density and low volume at the tip of the funnel; and, on the contrary, a low density and high volume at the opening edge. The Markov chain typically explores the opening edge but fails to go down the funnel because of the high curvature ([Neal, 2003](#); [Betancourt and Girolami, 2013](#)). As a result, the posterior sample may have significant bias and the subsequent inference

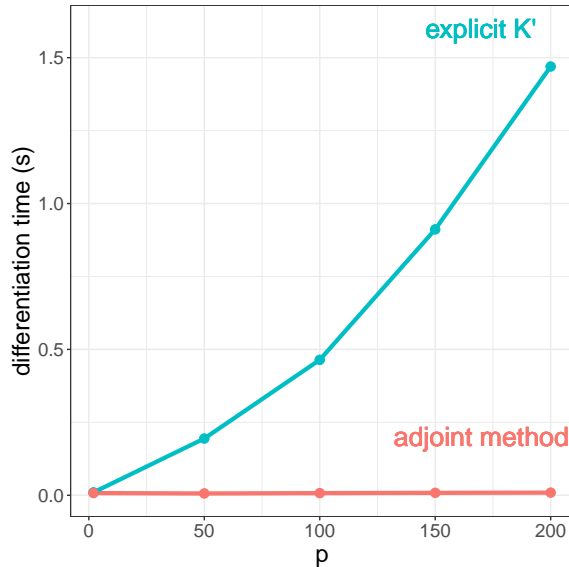


FIG 3. Wall time to differentiate the marginal log density. Algorithm 2 explicitly computes the tensor of derivatives K' , an operation that becomes costly as the dimension of the hyperparameter, p , increases. Algorithm 3 only computes $w^T K'$, where w is the cotangent vector prescribed by Theorem 1.

is unreliable. Fortunately, this failure can, with HMC, manifest itself as *divergent transitions*.

A standard practice to remedy the above problem is to use a *non-centered parameterization*, based on the equivalent data generating process

$$\begin{aligned}
 (\rho, \alpha) &\sim \pi(\rho, \alpha) \\
 z &\sim \text{Normal}(0, I_{n \times n}) \\
 L &= \text{Cholesky decompose}(K) \\
 \theta &= Lz \\
 y_i &\sim \text{Poisson}(y_e^i e^{\theta_i}).
 \end{aligned}$$

The Markov chain now operates on ρ , α , and z . This strategy often works, but in the example at hand, the geometry still poses challenges for HMC.

We can take a further step by adjusting the *adapt delta*, δ_a , tuning parameter of dynamic HMC. Broadly speaking, δ_a controls the numerical precision with which we compute Hamiltonian trajectories with the usual trade-off between accuracy and speed. The optimal value for constant curvature, and default in Stan, is 0.8 (Betancourt, Byrne and Girolami, 2015). When faced with divergent transitions, one strategy is to increase δ_a closer to 1. In the experiments for this paper, we increase it to 0.99.

An immediate benefit of the embedded Laplace approximation is that we marginalize out θ and only run HMC on α and ρ , a two-dimensional and typically well behaved parameter space. In the case of the disease map, we do not need to reparameterize the model, nor adjust δ_a .

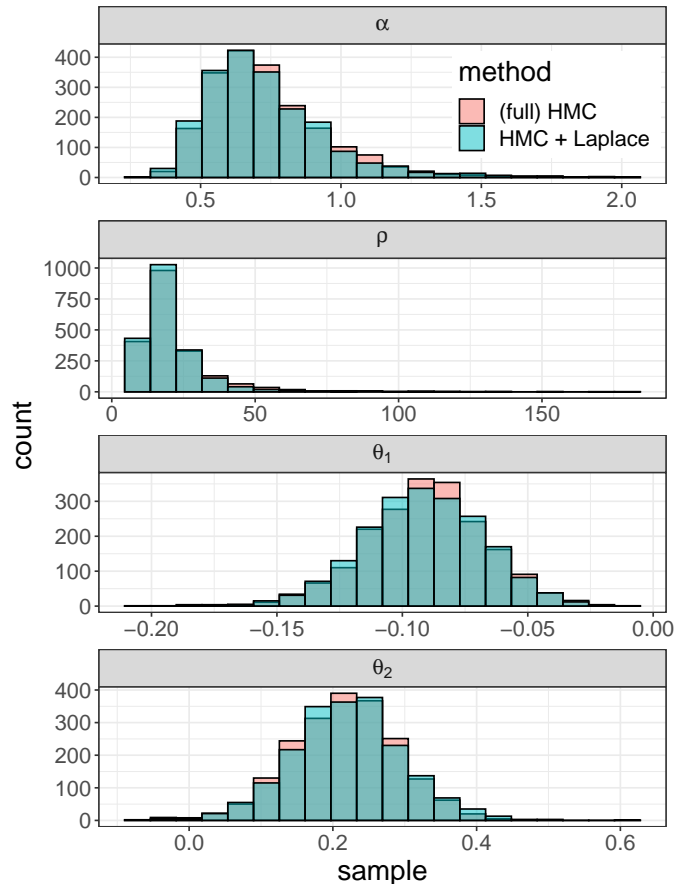


FIG 4. Samples obtained with full HMC and HMC using an embedded Laplace approximation when fitting the disease map Gaussian process. In this example, the samples generated by the two methods are in close agreement.

We fit two models, with 4 parallel chains, each with 500 warmup and 500 sampling iterations. The first model uses full HMC and a non-centered parameterization. When $\delta_a = 0.8$ we get 30 divergent transitions. When $\delta_a = 0.99$, we get no divergent transition, suggesting the sample is unbiased. The second model couples HMC with the embedded Laplace approximation, and simulates θ after doing the MCMC sampling⁵. With $\delta_a = 0.8$ the model returns no divergent transition. A look at the marginal distributions of α , ρ , and the first two elements of θ suggests the posterior samples generated by the two procedures are in close agreement (Figure 4). This is consistent with the more detailed analysis by Vanhatalo, Pietiläinen and Vehtari (2010) who demonstrate the error introduced by the Laplace approximation is small when using a Poisson or negative binomial likelihood.

To evaluate the efficiency of each model, we examine

⁵In Stan, this is done in the generated quantities block.

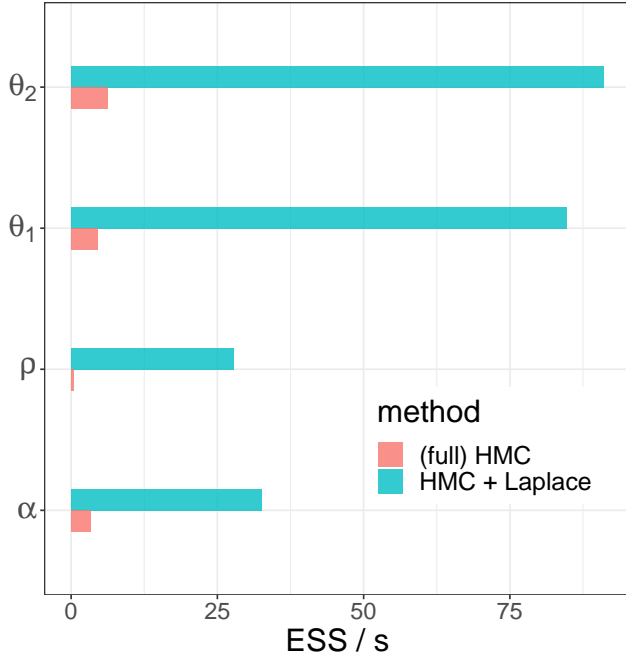


FIG 5. Bulk effective sample size per second. Coupling dynamic HMC with the embedded Laplace approximation yields a considerable speed-up when fitting a Gaussian process.

the bulk effective sample size (ESS), which constitutes an improvement over the traditional effective sample size (Vehetari et al., 2020). Conceptually, the ESS tells us the information contained in our MCMC sample, when estimating bulk quantities, e.g. medians and expectation values, is equivalent to the information contained in ESS independent draws from the posterior. Because the Markov chain samples are correlated, ESS is typically smaller than the total number of samples. The ESS acts as a proxy for the error in our Monte Carlo estimates and assumes that estimates are unbiased. Hence it does not account for the bias the Laplace approximation introduces. In this example, the bias is negligible but for other problems, the utility of the ESS per second (ESS/s) as a measure of efficiency may be, for this and other reasons, limited.

Figure 5 shows that, looking at the ESS/s, the embedded Laplace approximation yields a significant gain in efficiency.

4. GENERAL LINEAR REGRESSION MODELS WITH A HORSESHOE PRIOR

Consider a model with n observations and p covariates. In the “ $p \gg n$ ” regime, we can use sparsity inducing priors. The *horseshoe prior* (Carvalho, Polson and Scott, 2010) is a sparsity inducing prior useful when it is assumed that only a small portion of the regression coefficients are

significantly non-zero. Here we use the regularized horseshoe prior by Piironen and Vehtari (2017). The horseshoe prior is parameterized by a global regularization term, the scalar τ , and local regularization terms for each covariate, λ . Consequently the number of hyperparameters is $\mathcal{O}(p)$.

The data generating process is

$$\begin{aligned} \phi &\sim \pi(\phi) \\ \beta_0 &\sim \text{Normal}(0, c_0^2) \\ \beta &\sim \text{Normal}(0, \Sigma(\phi)) \\ y &\sim \text{Bernoulli_logit}(\beta_0 + X\beta), \end{aligned}$$

or, recasting it as a latent Gaussian model,

$$\begin{aligned} \phi &\sim \pi(\phi) \\ \theta &\sim \text{Normal}(0, c_0^2 I_{n \times n} + X\Sigma(\phi)X^T) \\ y &\sim \text{Bernoulli_logit}(\theta). \end{aligned}$$

When using HMC alone, the first formulation is computationally better because it avoids the expensive evaluation and differentiation of $K = c^2 I_{n \times n} + X\Sigma(\phi)X^T$. The embedded Laplace approximation requires the second formulation. The main benefit of the Laplace approximation is therefore not an immediate speed-up but an improved posterior geometry, due to marginalizing θ out. This means we do not need to fine tune the sampler to successfully sample from the posterior.

To see this, we examine the microarray classification data set on prostate cancer used by Piironen and Vehtari (2017). Here, $n = 102$ and $p = 5966$. We use 1000 iterations to warm up our sampler and 12000 sampling iterations over 6 chains; that is, 6 chains with 1000 warmup iterations and 2000 sampling iterations each. For this model we are interested in tail quantiles, such as the 90th quantile, as they allow us to identify parameters which have a small local shrinkage and thence relevant covariates. The large number of posterior draws is meant to reduce the variance of Monte Carlo estimates for such quantiles.

4.1 Fitting the model with full Hamiltonian Monte Carlo

This section describes how to tune (full) dynamic HMC to fit the model at hand. Some of the details may be cumbersome to the reader. But the takeaway is simple: tuning the algorithm is hard and can be a real burden for the modeler.

For full HMC, we use a non-centered parameterization. With Stan’s default parameters, we obtain ~ 150 divergent transitions⁶. As before, we increase adapt delta to $\delta_a = 0.99$ but find the sampler now produces 186 divergent transitions. A closer inspection reveals the divergences all

⁶ To be precise, we here did a preliminary run using 4000 sampling iterations and obtained 50 divergent transitions (so an expected 150 over 12000 sampling iterations).

Chain	Step size	Acceptance rate	Divergences
1	0.0065	0.99	0
2	0.0084	0.90	186
3	0.0052	0.99	0
4	0.0061	0.99	0

TABLE 1

Adapted tuning parameters across 4 Markov chains with $\delta_a = 0.99$.

come from a single chain, which also has a larger adapted step size, δ (table 1).

It is worth reviewing the role of δ in the algorithm. A more comprehensive discussion can be found in the papers by Betancourt (2018a) and Hoffman and Gelman (2014). To run HMC, we need to numerically compute physical trajectories by solving the system of differential equations prescribed by Hamilton’s equations of motion. We do this using a numerical integrator. A small step size, δ , makes the integrator more precise but generates smaller trajectories, which leads to a less efficient exploration of the parameter space. When we introduce too much numerical error, the proposed trajectory is rejected. Adapt delta, $\delta_a \in (0, 1)$, sets the target acceptance rate of proposed trajectories. During the warmup, the sampler adjusts δ to meet this target.

The problematic chain produces a large δ and fails to achieve the target acceptance rate. Table 1 provides the result for the failing chain and three “successful” chains. These results suggest increasing δ_a yet again may not provide any benefits. Instead we increase the final adaptation window during which the sampler tries to find the optimal step size from 50 iterations to 350 iterations (see Hoffman and Gelman, 2014; Stan development team, 2020). With this setup, we however obtain divergent transitions across all chains.

This outcome indicates the chains are relatively unstable and emphasizes how difficult it is, for this type of model and data, to come up with the right tuning parameters. With $\delta_a = 0.999$ and the expanded adaptation window we observe 13 divergent transitions. It is possible this result is the product of luck, rather than better tuning parameters. To be clear, we do not claim we found the optimal model parameterization and tuning parameters. There is however, to our knowledge, no straightforward way to do so. While this outcome is not ideal we choose to rely on it in our benchmark study, because the number of divergences is relatively low and the chains (with or without divergent transitions) produce consistent results.

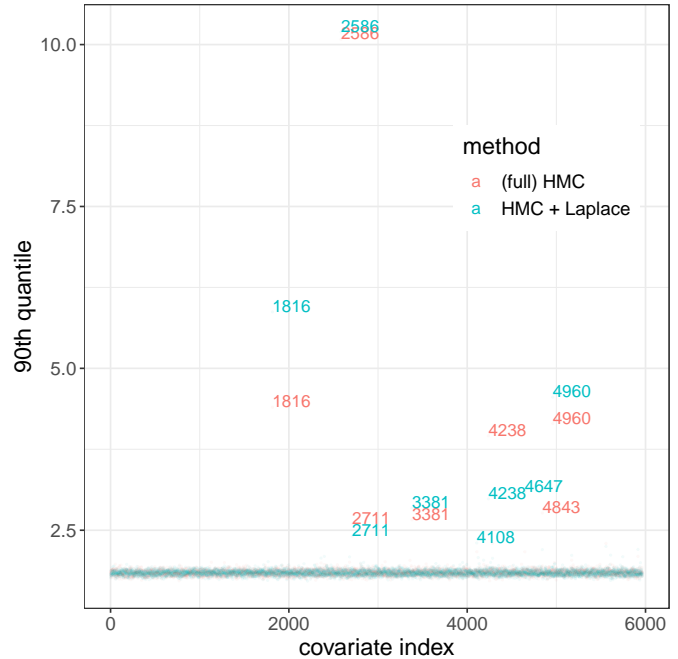


FIG 6. 90th quantile for $\log \lambda$ across all covariates for the general linear model with a horseshoe prior.

(full) HMC	2586	1816	4960	4238	4843	3381
HMC						
+ Laplace	2586	1816	4960	4647	4238	3381

TABLE 2

Ordered covariate indices with the highest 90th quantiles for the general linear model with a horseshoe prior.

4.2 Fitting the model with the embedded Laplace approximation

Running the algorithm with Stan’s default tuning parameters produces 0 divergent transitions over 12000 sampling iterations.

4.3 Evaluation and Comparison

We identify the most relevant covariates by examining the distribution of λ . If the i^{th} covariate is strongly explanatory, $\pi(\lambda_i | \mathcal{D})$ puts probability mass at high values, meaning little regularization beyond what we have from the global shrinkage term, τ , occurs. In such an instance, $\pi(\lambda_i | \mathcal{D})$ may be bimodal and typically has a large 90th quantile. Figure 6 and table 2 show the covariates “softly selected” by the model when fitted with full HMC and with HMC with an embedded Laplace approximation.

As with the Gaussian process, we look at the distributions of hyperparameters. We confine our attention to τ , the global shrinkage, c_{aux} , the slab parameter, and λ

for the 2586th and 1816th covariates, as these seem to be the most relevant ones. Figure 7 plots a histogram of the posterior draws (for clarity we use the logarithmic scale) and Figure 8 compares the estimated probabilities of developing prostate cancer. The Laplace approximation introduces an error, yielding less extreme probabilities of having or not having cancer. This behavior is expected for latent Gaussian models with a Bernoulli observation model, and has been studied in the cases of Gaussian processes and Gaussian random Markov fields (e.g. Kuss and Rasmussen, 2005; Botond and Heskes, 2011; Vehtari et al., 2016).

We next plot the ESS / s (Figure 9) but we point out two caveats. First with a Bernoulli likelihood, the Laplace approximation introduces a bias, as notably evidenced by Figures 7 and 8, and as reported in the cited literature. The ESS is only a proxy for the variance of the Monte Carlo estimators, not the complete error. Whether the bias is significant or not depends on the quantities of interest and the desired precision. Secondly this measure of efficiency does not account for the fact we had to fit the model multiple times in order to tune full HMC, while it sufficed to run the embedded Laplace approximation only once.

5. SPARSE KERNEL INTERACTION MODEL

A natural extension of the general linear regression is to include interaction terms. To achieve better computational scalability, we can use the *kernel interaction trick* by Agrawal et al. (2019) and build a *sparse kernel interaction model* (SKIM), which also uses the regularized horseshoe prior by Piiroinen and Vehtari (2017). The model is an explicit latent Gaussian model and uses a non-trivial covariance matrix. The full details of the model are exposed in Appendix C.2.

This example demonstrates the wide range of models users may be interested in and further motivates the need for a flexible probabilistic programming language that allows practitioners to specify their covariance matrix, without burdening them to work out derivatives by hand. In this setting, we have once again a high dimensional hyperparameter and a potentially multi-modal posterior distribution. Unlike the general linear model, the covariance matrix must be explicitly constructed with both full HMC and HMC with an embedded Laplace approximation.

When fitting the SKIM to the prostate cancer data, we encounter similar challenges as in the previous section: ~ 150 divergent transitions with full HMC. The behavior when adding the embedded Laplace approximation is better, though we do pick up ~ 3 divergent transitions⁷. We

⁷ We do our preliminary runs using only 4000 sampling iterations. The above number are estimated for 12000 sampling iterations. The same holds for the estimated run times.

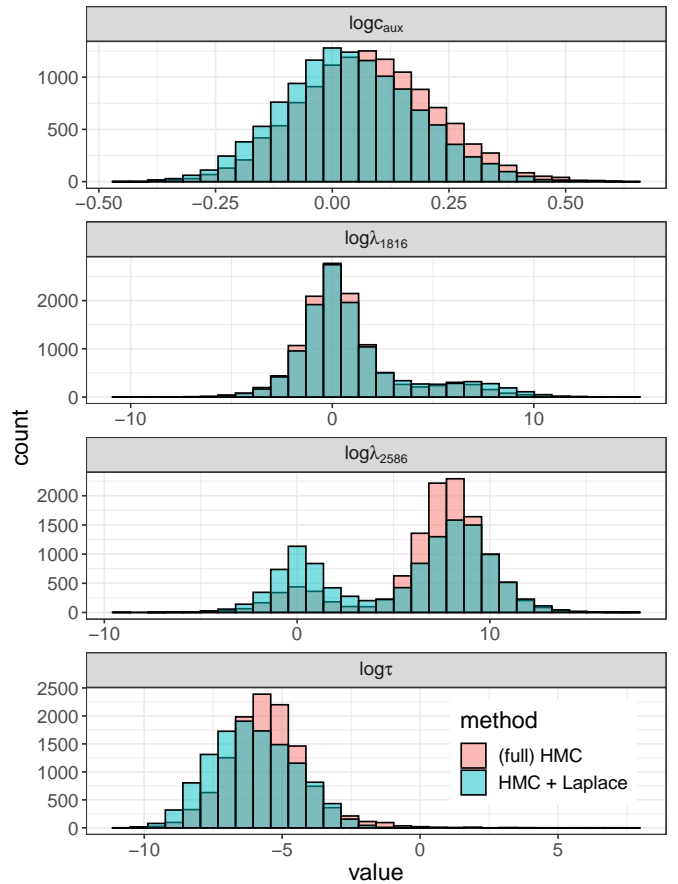


FIG 7. Samples for the general linear regression model with a horseshoe prior.

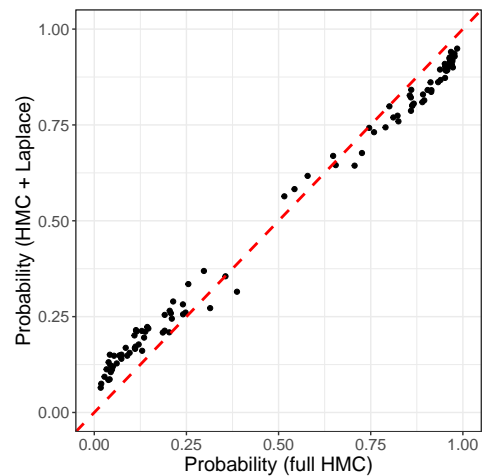


FIG 8. Expectation value for the probability of developing prostate cancer, as estimated by full HMC and HMC using an embedded Laplace approximation.

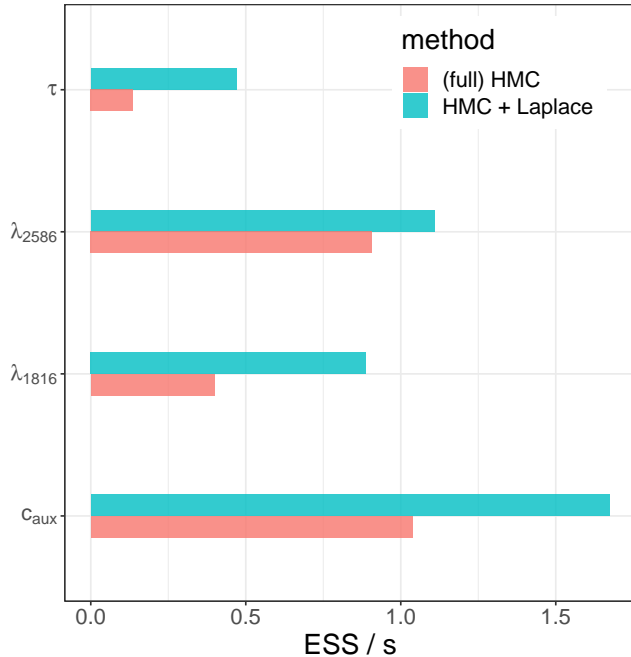


FIG 9. Bulk effective sample size per second for general linear model with a regularizing horseshoe prior.

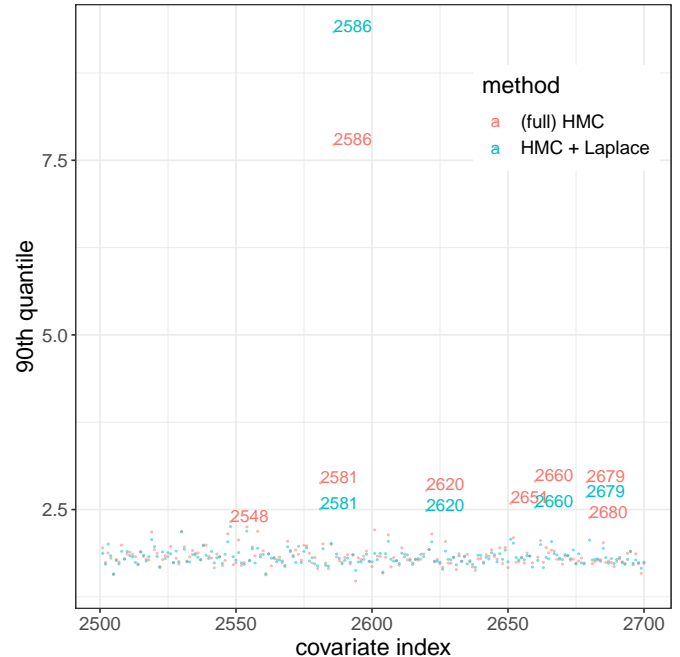


FIG 10. 90th quantiles for $\log \lambda$ across all covariates in the sparse kernel interaction model.

also find large differences in running time. The embedded Laplace approximation runs for ~ 10 hours, while full HMC takes ~ 20 hours with $\delta_a = 0.8$ and ~ 50 hours with $\delta_a = 0.99$, making it difficult to tune the sampler and run our computer experiment.

For computational convenience, we fit the SKIM using only 200 covariates, indexed 2500 - 2700 to encompass the 2586th covariate which we found to be strongly explanatory. This allows us to easily tune full HMC without altering the takeaways of the experiment. Note the data here used is different from the data we used in the previous section (since we only examine a subset of the covariates) and the marginal posteriors should therefore not be compared directly.

As above, we run 6 chains with combined 12000 iterations. For full HMC we obtain 36 divergent transitions with $\delta_a = 0.8$ and 0 with $\delta_a = 0.99$. The embedded Laplace approximation produces 0 divergences with $\delta_a = 0.8$. Figures 10 and Figure 11 compare posterior draws, while Figure 12 plots the ESS/s of both methods.

6. DISCUSSION

Equipped with a scalable differentiation algorithm, we expand the regime of models to which we can apply the embedded Laplace approximation. By coupling the approximation with HMC, we can now fit models with high dimensional hyperparameters, ϕ , and a multimodal poste-

rior distribution, provided the energy barrier is not too strong. The main benefit of marginalizing out the latent Gaussian parameter, θ , is to improve the geometry of the posterior distribution, as notably manifested by a decrease in divergent transitions. The added geometric stability has two benefits: (i) we do not need to tune the HMC sampler which can require a substantial effort from the modeler, and (ii) the effective sample size per second of the sampler is higher.

Our recommendation is to use the embedded Laplace approximation when the dimension of the latent Gaussian parameter, θ , is much higher than that of the hyperparameter, ϕ , or when the joint posterior geometry exhibits high and uneven curvature. In the latter case, even when θ is low dimensional (relative to ϕ), marginalizing θ out alleviates geometric difficulties. If on the other hand the posterior is well-behaved, the benefits of the embedded Laplace approximation are marginal. For example, we find that fitting the ovarian cancer data in Piironen and Vehtari (2017) works better with full HMC, because we see no divergent transitions with Stan’s default tuning parameters and we do not need to compute the full covariance matrix of θ . For the SKIM, the efficiency of both methods is on par when the posterior is well behaved.

The immediate next step is to further develop the prototype in Stan, so that researchers may experiment more with the method. Beyond that, the current prototype does not use many features that allow a high performance

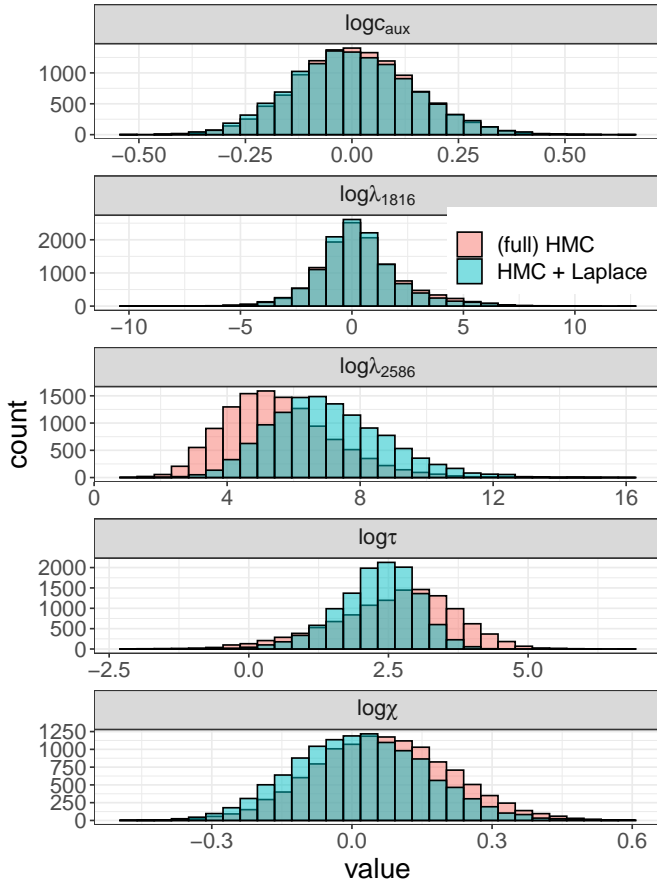


FIG 11. Posterior samples for the sparse kernel interaction model.

implementation of the Laplace approximation, as seen in the packages INLA, TMB, and GPstuff. Examples include: support for sparse matrices required to efficiently fit latent Markov random field models, parallelization across cores and GPUs, and persistent initial guesses for the Newton solver. Much of these features exist in Stan and can be carried over.

We also want to improve the flexibility of the method by allowing users to specify their own likelihood. In this respect, the implementation in TMB is exemplary. The main computational bottle neck is evaluating the third-order derivatives of the likelihood. It is in principle possible to apply automatic differentiation to do higher-order automatic differentiation and most libraries, including Stan, support this; but, along with feasibility, there is a question of efficiency and practicality (e.g [Betancourt, 2018b](#)). To what extent can higher-order automatic differentiation support an efficient embedded Laplace approximation? This depends on the likelihood. A challenging example thereof would be likelihoods that depend on the implicit solution to ordinary differential equations, as often seen

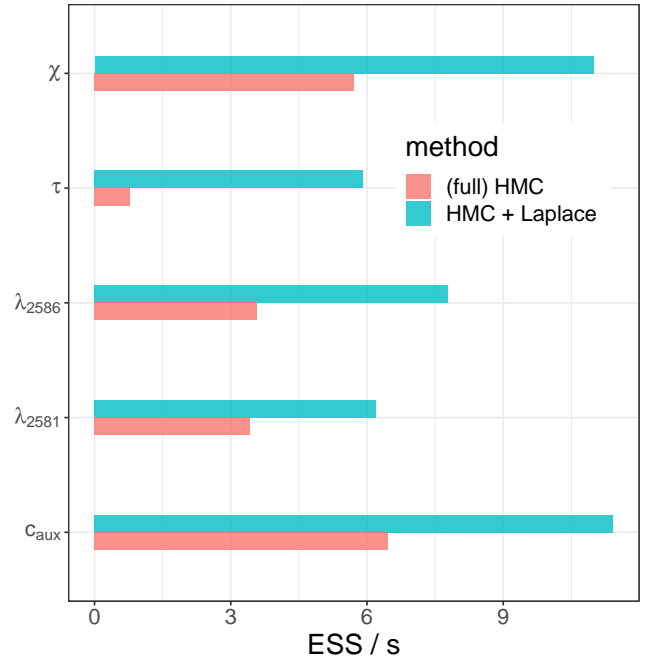


FIG 12. Bulk effective sample size per second for hyperparameters of the sparse kernel interaction model.

in the natural sciences.

Along with the added flexibility comes the burden of more robustly diagnosing errors induced by the approximation. There is extensive literature on log-concave likelihoods but less so for general likelihoods. Future work will investigate diagnostics such as importance sampling ([Vehtari et al., 2019](#)), leave-one-out cross-validation ([Vehtari et al., 2016](#)), and simulation based calibration ([Talts et al., 2018](#)).

7. ACKNOWLEDGMENT

We thank Michael Betancourt, Steve Bronder, Alejandro Catalina, Rok Češnovar, Sam Power, and Sean Talts for helpful discussions.

CM thanks the Office of Naval Research, the National Science Foundation, the Institute for Education Sciences, and the Sloan Foundation. CM and AV thank the Academy of Finland (grants 298742 and 313122). DS thanks the Canada Research Chairs program and the Natural Sciences and Engineering Research Council of Canada. RA’s research was supported in part by a grant from DARPA.

We acknowledge computing resources from Columbia University’s Shared Research Computing Facility project, which is supported by NIH Research Facility Improvement Grant 1G20RR030893-01, and associated funds from the New York State Empire State Development, Division of

Science Technology and Innovation (NYSTAR) Contract C090171, both awarded April 15, 2010.

We also acknowledge the computational resources provided by the Aalto Science-IT project.

REFERENCES

- AGRAWAL, R., HUGGINS, J. H., TRIPPE, B. and BRODERICK, T. (2019). The Kernel Interaction Trick: Fast Bayesian Discovery of Pairwise Interactions in High Dimensions. *Proceedings of the 36th International Conference on Machine Learning* **97**.
- BAYDIN, A. G., PEARLMUTTER, B. A., RADUL, A. A. and SISKIND, J. M. (2018). Automatic differentiation in machine learning: a survey. *Journal of Machine Learning Research* **18** 1 – 43.
- BELL, B. M. and BURKE, J. V. (2008). Algorithmic Differentiation of Implicit Functions and Optimal Values. In *Advances in Automatic Differentiation. Lecture Notes in Computational Science and Engineering*, (C. H. Bischof, H. M. Bücker, P. Hovland, U. Naumann and J. Utke, eds.) **64** Springer, Berlin, Heidelberg.
- BETANCOURT, M. (2018a). A Conceptual Introduction to Hamiltonian Monte Carlo. *arXiv:1701.02434v1*.
- BETANCOURT, M. (2018b). A Geometric Theory of Higher-Order Automatic Differentiation. *arXiv:1812.11592*.
- BETANCOURT, M., BYRNE, S. and GIROLAMI, M. (2015). Optimizing the integrator step size of Hamiltonian Monte Carlo. *arXiv:1411.6669*.
- BETANCOURT, M. and GIROLAMI, M. (2013). Hamiltonian Monte Carlo for Hierarchical Models. *arXiv:1312.0906v1*.
- BETANCOURT, M. J., BYRNE, S., LIVINGSTONE, S. and GIROLAMI, M. (2017). The Geometric Foundations of Hamiltonian Monte Carlo. *Bernoulli* **23** 2257 – 2298.
- BOTOND, C. and HESKES, T. (2011). Approximate marginals in latent Gaussian models. *Journal of Machine Learning Research* **12**.
- CARPENTER, B., HOFFMAN, M. D., BRUBAKER, M. A., LEE, D., LI, P. and BETANCOURT, M. J. (2015). The Stan Math Library: Reverse-Mode Automatic Differentiation in C++. *arXiv 1509.07164*.
- CARPENTER, B., GELMAN, A., HOFFMAN, M., LEE, D., GOODRICH, B., BETANCOURT, M., BRUBAKER, M. A., GUO, J., LI, P. and RIDDEL, A. (2017). Stan: A Probabilistic Programming Language. *Journal of Statistical Software* **76** 1–32.
- CARVALHO, C. M., POLSON, N. G. and SCOTT, J. G. (2010). The horseshoe estimator for sparse signals. *Biometrika* **97** 465–480.
- STAN DEVELOPMENT TEAM (2020). *Stan reference manual*.
- ERRICO, M. (1997). What is an adjoint model? *Bulletin of the American Meteorological Society* **78** 2577 – 2591.
- GÓMEZ-RUBIO, V. and RUE, H. (2018). Markov chain Monte Carlo with the Integrated Nested Laplace Approximation. *Statistics and Computing* **28** 1033 – 1051.
- GRIEWANK, A. and WALTHER, A. (2008). *Evaluating derivatives*, Second ed. Society for Industrial and Applied Mathematics (SIAM), Philadelphia, PA.
- HOFFMAN, M. D. and GELMAN, A. (2014). The No-U-Turn Sampler: Adaptively Setting Path Lengths in Hamiltonian Monte Carlo. *Journal of Machine Learning Research* **15** 1593–1623.
- KRISTENSEN, K., NIELSEN, A., BERG, C. W., SKAUG, H. and BELL, B. M. (2016). TMB: Automatic Differentiation and Laplace Approximation. *Journal of statistical software* **70** 1 – 21.
- KUSS, M. and RASMUSSEN, C. E. (2005). Assessing Approximate Inference for Binary Gaussian Process Classification. *Journal of Machine Learning Research* **6** 1679 – 1704.
- MARGOSSIAN, C. C. (2019). A Review of automatic differentiation and its efficient implementation. *Wiley interdisciplinary reviews: data mining and knowledge discovery* **9**.
- MONNAHAN, C. C. and KRISTENSEN, K. (2018). No-U-turn sampling for fast Bayesian inference in ADMB and TMB: Introducing the admn and tmbstan R packages. *Plos One* **13**.
- NEAL, R. M. (2003). Slice sampling. *Annals of statistics* **31** 705 – 767.
- NEAL, R. M. (2012). MCMC using Hamiltonian Dynamics. In *Handbook of Markov Chain Monte Carlo* Chapman & Hall / CRC Press.
- PIIRONEN, J. and VEHTARI, A. (2017). Sparsity information and regularization in the horseshoe and other shrinkage priors. *Electronic Journal of Statistics* **11** 5018–5051.
- RASMUSSEN, C. E. and WILLIAMS, C. K. I. (2006). *Gaussian Processes for Machine Learning*. The MIT Press.
- RUE, H. and CHOPIN, N. (2009). Approximate Bayesian inference for latent Gaussian models by using integrated nested Laplace approximations. *Journal of Royal Statistics B* **71** 319 – 392.
- RUE, H., RIEBLER, A., SORBYE, S., ILLIAN, J., SIMSON, D. and LINDGREN, F. (2017). Bayesian Computing with INLA: A Review. *Annual Review of Statistics and its Application* **4** 395 – 421.
- SALVATIER, J., WIECKI, T. V. and FONNESBECK, C. (2016). Probabilistic programming in Python using PyMC3. *PeerJ Computer Science* **2**.
- TALTS, S., BETANCOURT, M., SIMPSON, D., VEHTARI, A. and GELMAN, A. (2018). Validating Bayesian inference algorithms with simulation-based calibration. *arXiv:1804.06788v1*.
- TIERNEY, L. and KADANE, J. B. (1986). Accurate Approximations for Posterior Moments and Marginal Densities. *Journal of the American Statistical Association* **81** 82–86.
- VANHATALO, J., PIETILÄINEN, V. and VEHTARI, A. (2010). Approximate inference for disease mapping with sparse Gaussian processes. *Statistics in Medicine* **29** 1580–1607.
- VANHATALO, J., RIIHIMÄKI, J., HARTIKAINEN, J., JYLÄNKI, P., TOLVANEN, V. and VEHTARI, A. (2013). GPstuff: Bayesian Modeling with Gaussian Processes. *Journal of Machine Learning Research* **14** 1175–1179.
- VEHTARI, A., MONONEN, T., TOLVANEN, V., SIVULA, T. and WINTHER, O. (2016). Bayesian Leave-One-Out Cross-Validation Approximations for Gaussian Latent Variable Models. *Journal of Machine Learning Research* **17** 1–38.
- VEHTARI, A., SIMPSON, D., GELMAN, A., YAO, Y. and GABRY, J. (2019). Pareto smoothed importance sampling. *arXiv:1507.02646*.
- VEHTARI, A., GELMAN, A., SIMPSON, D., CARPENTER, B.

and BUERKNER, P.-C. (2020). Rank-normalization, folding, and localization: An improved \hat{R} for assessing convergence of MCMC. *arXiv:1903.08008*.

APPENDIX A: DETAILS FOR THE ADJOINT METHOD

This appendix fills the gap in Section 2.4 and offers a proof of Theorem 1. As a starting point, we assume Algorithm 2 is valid. A proof can be found in Rasmussen and Williams (2006), chapter 5.

The key observation is that all operations performed on

$$(K')_j := \frac{\partial K}{\partial \phi_j}$$

are linear. Algorithm 2 produces a map

$$\begin{aligned} \mathcal{Z} &: (K')_j \rightarrow \frac{\partial}{\partial \phi_j} \pi(y | \phi) \\ &: \mathbb{R}^{n \times n} \rightarrow \mathbb{R}, \end{aligned}$$

and constructs the gradient one element at a time. By linearity,

$$\frac{\partial}{\partial \phi_j} \mathcal{Z}(K) = \mathcal{Z} \left(\frac{\partial K}{\partial \phi_j} \right).$$

Thus an alternative approach to compute the gradient is to calculate the scalar $\mathcal{Z}(K)$ and then use a single reverse mode sweep of automatic differentiation, noting that \mathcal{Z} is an analytical function. This produces Algorithm 4. At

Algorithm 4 *Approximate gradient of the marginal likelihood, $\pi(y | \phi)$, with respect to the hyperparameters, ϕ , using reverse mode automatic differentiation*

input: $y, \phi, \pi(y | \theta, \phi)$

2: Do lines 2 - 6 of Algorithm 2.

Initiate an expression tree for automatic differentiation with $\phi_v = \phi$.

4: $K_v = \mathcal{K}(\phi_v)$

$z = \mathcal{Z}(K_v)$

6: Do a reverse-sweep over z to obtain $\nabla_\phi \log \pi(y | \phi)$.

return: $\nabla_\phi \log \pi(y | \phi)$.

this point, the most important is done in order to achieve scalability: we no longer explicitly compute K' and are using a single reverse mode sweep. Automatic differentiation, for all its relatively cheap cost, still incurs some overhead cost. Hence, where possible, we still want to use analytical results to compute derivatives. In particular, we can analytically work out the cotangent

$$w^T := \frac{\partial z}{\partial K}.$$

For the following calculations, we use a lower case, k_{ij} and r_{ij} , to denote the $(ij)^{\text{th}}$ element respectively of the matrices K and R .

Consider

$$\mathcal{Z}(K) = s_1 + s_2^T s_3,$$

where, unlike in Algorithm 2, s_1 and s_3 are now computed using K , not $(K')_j$. We have

$$s_1 = \frac{1}{2} a^T K a - \frac{1}{2} \text{tr}(RK).$$

Then

$$\frac{\partial}{\partial k_{i'j'}} a^T K a = \frac{\partial}{\partial k_{i'j'}} \sum_i \sum_j a_i k_{ij} a_j = a_{i'} a_{j'},$$

and

$$\frac{\partial}{\partial k_{i'j'}} \text{tr}(RK) = \frac{\partial}{\partial k_{i'j'}} \sum_l r_{il} k_{li} = r_{j'i'}.$$

Thus

$$\frac{\partial s_1}{\partial K} = \frac{1}{2} a a^T - \frac{1}{2} R^T.$$

For convenience, denote $l = \nabla_\theta \log \pi(y | \theta, \phi)$. We then have

$$b = Kl$$

$$s_3 = b - \tilde{K} R b = (I - \tilde{K} R) b,$$

where $\tilde{K} = K$, but is maintained fixed, meaning we do not propagate derivatives through it. Let $\tilde{A} = I - \tilde{K} R$ and let \tilde{a}_{ij} denote the $(i, j)^{\text{th}}$ element of \tilde{A} . Then

$$s_2^T s_3 = \sum_i (s_2)_i \left(\sum_j \tilde{a}_{ij} \sum_m k_{jm} l_m \right).$$

Thus

$$\frac{\partial}{\partial k_{i'j'}} s_2^T s_3 = \sum_i (s_2)_i \tilde{a}_{ii'} l_{j'} = l_{j'} \sum_i (s_2)_i \tilde{a}_{ii'},$$

where the sum term is the $(i')^{\text{th}}$ element of $\tilde{A} s_2$. The above expression then becomes

$$\frac{\partial}{\partial K} s_2^T s_3 = \tilde{A} s_2 l^T = s_2 l^T - K R s_2 l^T.$$

Combining the derivative for s_1 and $s_2^T s_3$ we obtain

$$w^T = \frac{1}{2} a a^T - \frac{1}{2} R + (s_2 + R K s_2) [\nabla_\theta \log \pi(y | \theta, \phi)]^T,$$

as prescribed by Theorem 1. This result is general, in the sense that it applies to any covariance matrix, K , and likelihood, $\pi(y | \theta, \phi)$.

Our preliminary experiments, on the SKIM, found that incorporating the analytical cotangent, w^T , approximately doubles the differentiation speed.

APPENDIX B: COMPUTER CODE

The code used in this work is open source and detailed in this section.

B.1 Prototype Stan code

The Stan language allows users to specify the joint log density of their model. This is done by incrementing the variable `target`. We add a suite of functions, which return the approximate log marginal density, $\log \pi_G(y | \phi)$. Hence, the user can specify the log joint distribution by incrementing `target` with $\log \pi_G(y | \phi)$ and the prior $\log \pi(\phi)$. A call to the approximate marginal density may look as follows:

```
target +=
  laplace_marginal_*(y, n, K, phi, x,
                    delta, delta_int,
                    theta0);
```

The `*` specifies the likelihood, for example Bernoulli or Poisson⁸. `y` and `n` are sufficient statistics for the latent Gaussian variable, θ ; `K` is a function that takes in arguments `phi`, `x`, `delta`, and `delta_int` and returns the covariance matrix; and `theta0` is the initial guess for the Newton solver, which seeks the mode of $\pi(\theta | \phi, y)$. Specifically

- `y`: a vector containing the sum of counts/successes for each element of θ
- `n`: a vector with the number of observation for each element of θ
- `K`: a function defined in the functions block, with the signature `(vector, matrix, real[], int[]) ==> matrix`
- `phi`: the vector of hyperparameters
- `x`: a matrix of data. For Gaussian processes, this is the coordinates, and for the general linear regression, the design matrix.
- `delta`: additional real data.
- `delta_int`: additional integer data.
- `theta0`: a vector of initial guess for the Newton solver.

It is also possible to specify the tolerance of the Newton solver. This structure is consistent with other higher-order functions in Stan, such as the algebraic solver and the ordinary differential equation integrators. It gives users

⁸ These are the current options in the prototype we used in this article; the immediate next version also specifies the link function.

flexibility when specifying K , but we recognize it is cumbersome. The Stan development team has, for another project, a prototype that relaxes the strict function signature requirement, which we plan to take advantage of.

For each likelihood, we implement a corresponding random number generating function, with a call

```
theta =
  laplace_marginal_*_rng(y, n, K, phi, x,
                        delta, delta_int,
                        theta0);
```

This generates a random sample from $\pi_G(\theta | y, \phi)$. This function can be used in the generated quantities blocks and is called only once per iteration – in contrast with the target function which is called and differentiated once per integration step of HMC. Moreover the cost of generating θ is negligible next to the cost evaluating and differentiating $\log \pi(y | \phi)$ multiple times per iteration.

B.2 Core code for Stan

We incorporate the Laplace suite of functions inside the Stan-math library, a C++ library for automatic differentiation (Carpenter et al., 2015). The library is open source and available on GitHub, <https://github.com/stan-dev/math>. Our prototype exists on the branch `try-laplace_approximation`.

To expose the code to the Stan language, we use Stan’s new OCaml transpiler, `stanc3`, <https://github.com/stan-dev/stanc3> and again the branch `try-laplace_approximation`.

B.3 Code for the computer experiment

The R code is available on the GitHub public repository, https://github.com/charlems93/laplace_manuscript.

We make use of two new prototype packages: `CmdStanR` (<https://mc-stan.org/cmdstanr/>) and `posterior` (<https://github.com/jgabry/posterior>).

APPENDIX C: MODEL DETAILS

We review the models used in our computer experiments and point the readers to the relevant references.

C.1 Regularized horseshoe prior

The horseshoe prior (Carvalho, Polson and Scott, 2010) is a sparsity inducing prior that imposes a global shrinkage, τ , and a local shrinkage, λ_i for each covariate slope, β_i . This prior operates a soft variable selection, effectively favoring $\beta_i \approx 0$ or $\beta_i \approx \hat{\beta}_i$, where $\hat{\beta}_i$ is the maximum likelihood estimator. Piironen and Vehtari (2017) add another prior to regularize unshrunk β s, $\text{Normal}(0, c^2)$, effectively operating a “soft-truncation” of the extreme tails. For

computational stability, the model is parameterized using c_{aux} , rather than c , where

$$c = s_{\text{slab}} \sqrt{c_{\text{aux}}}$$

with s_{slab} the slab scale. We run MCMC over $\phi = (\tau, c_{\text{aux}}, \lambda)$ and the prior is

$$\begin{aligned} \lambda_i &\sim \text{Student}_t(\nu_{\text{local}}, 0, 1) \\ \tau &\sim \text{Student}_t(\nu_{\text{global}}, 0, s_{\text{global}}) \\ c_{\text{aux}} &\sim \text{inv}\Gamma(s_{\text{df}}/2, s_{\text{df}}/2) \\ \beta_0 &\sim \text{Normal}(0, c_0^2) \end{aligned}$$

The prior on λ independently applies to each element, λ_i .

Following the recommendation by [Piironen and Vehtari \(2017\)](#), we set the variables of the priors as follows. Let p be the number of covariates and n the number of observations. Additionally, let p_0 be the expected number of relevant covariates – note this number does not strictly enforce the number of unregularized β s, because the priors have heavy enough tails that we can depart from p_0 . For the prostate data, we set $p_0 = 5$. Then

$$\begin{aligned} s_{\text{global}} &= \frac{p_0}{\sqrt{n}(p - p_0)} \\ \nu_{\text{local}} &= 1 \\ \nu_{\text{global}} &= 1 \\ s_{\text{slab}} &= 2 \\ s_{\text{df}} &= 100 \\ c_0 &= 5. \end{aligned}$$

Next we construct the prior on β ,

$$\beta_i \sim \text{Normal}(0, \tau^2 \tilde{\lambda}_i^2),$$

where

$$\tilde{\lambda}_i^2 = \frac{c^2 \lambda_i^2}{c^2 + \tau^2 \lambda_i^2}.$$

The rest of the model is as dictated in Section 4.

C.2 Sparse kernel interaction model

SKIM, developed by [Agrawal et al. \(2019\)](#), extends the model of [Piironen and Vehtari \(2017\)](#) by accounting for pairwise interaction effects between covariates. The generative model shown below uses the notation in [C.1](#) instead of that in Appendix D of [Agrawal et al. \(2019\)](#):

$$\begin{aligned} \chi &\sim \text{inv}\Gamma(s_{\text{df}}/2, s_{\text{df}}/2) \\ \eta_2 &= \frac{\tau^2}{c^2} \chi \\ \beta_i \mid \tau, \tilde{\lambda} &\sim \text{Normal}(0, \tau^2 \tilde{\lambda}_i^2) \\ \beta_j \mid \tau, \tilde{\lambda} &\sim \text{Normal}(0, \tau^2 \tilde{\lambda}_j^2) \\ \beta_{ij} \mid \eta_2, \tilde{\lambda} &\sim \text{Normal}(0, \eta_2^2 \tilde{\lambda}_i^2 \tilde{\lambda}_j^2) \\ \beta_0 \mid c_0^2 &\sim \text{Normal}(0, c_0^2), \end{aligned}$$

where β_i and β_{ij} are the main and pairwise effects for covariates x_i and $x_i x_j$, respectively, and $\tau, \tilde{\lambda}, c_0$ are defined in [C.1](#).

Instead of sampling $\{\beta_i\}_{i=1}^p$ and $\{\beta_{ij}\}_{i,j=1}^p$, which takes at least $O(p^2)$ time per iteration to store and compute, [Agrawal et al. \(2019\)](#) instead marginalize out all the regression coefficients, only sampling $(\tau, \xi, \tilde{\lambda})$ via MCMC. Through a kernel trick and a Gaussian process re-parameterization of the model, this marginalization takes $O(p)$ time instead of $O(p^2)$. The Gaussian process covariance matrix K induced by SKIM is provided below:

$$\begin{aligned} K_1 &= x \text{diag}(\tilde{\lambda}^2) x^T \\ K_2 &= [x \circ x] \text{diag}(\tilde{\lambda}^2) [x \circ x]^T, \end{aligned}$$

where “ \circ ” denotes the element-wise Hadamard product. Finally,

$$\begin{aligned} K &= \frac{1}{2} \eta_2^2 (K_1 + 1) \circ (K_1 + 1) - \frac{1}{2} \eta_2^2 K_2 - (\tau^2 - \eta_2^2) K_1 \\ &\quad + c_0^2 - \frac{1}{2} \eta_2^2. \end{aligned}$$